Eur. J. Mineral.
2004, **16**, 387–399

Mechanical instability near the stishovite-$CaCl_2$ phase transition: implications for crystal preferred orientations and seismic properties

PATRICK CORDIER[1,2] DAVID MAINPRICE[3] and JED LEIGH MOSENFELDER[2,*]

[1]Laboratoire de Structure et Propriétés de l'Etat Solide, UMR CNRS 8008, Université des Sciences et Technologies de Lille, Bat C6, F-59655 Villeneuve d'Ascq, France
Corresponding author, e-mail: Patrick.Cordier@univ-lille1.fr
[2]Bayerisches Geoinstitut, Universität Bayreuth, D-95440 Bayreuth, Germany
*Currently at: Division of Geological and Planetary Sciences, California Institute of Technology, M/C 170-25 Pasadena, CA 91125
[3]Laboratoire de Tectonophysique, UMR CNRS 5866, Université Montpellier II, France

Abstract: Deformation experiments have been performed on polycrystalline stishovite at 14 GPa and 1300 °C in a multi-anvil press. The easy slip systems have been determined by Transmission Electron Microscopy. We found [001]{100} and [001]{110} with minor slip in the <100> direction. Analysis of the elastic energy of these slip systems together with previously reported systems in as-grown stishovite reveals that easy glide [001]{100} and [001]{110} systems are unaffected by the stishovite to $CaCl_2$ transformation, whereas the energy of <110>{1$\bar{1}$0} system decreases to zero at the transition, which is symptomatic of a plastic instability.

We have used the visco-plastic self-consistent (VPSC) model to simulate the crystal preferred orientation (CPO) of polycrystalline stishovite in simple shear. The CPO in stishovite stability field shows a strong alignment of [001] axes parallel to direction of maximum finite strain (X) and a girdle of [100] normal to X. At conditions close to the transition, simulated by making the CRSS of [110](1$\bar{1}$0) equal to easy glide [001] systems, the CPO were similar to the previous case, but slightly weaker. At the transition, simulated by making the <110>{1$\bar{1}$0} systems the only easy glide systems, the CPO of [001] axes is very weak.

The anisotropic seismic properties were calculated from the CPO. In the stishovite stability field at a pressure of 21 GPa the Vp maximum is parallel to X and Vp minimum parallel to Z with an anisotropy of about 13%. The shear wave splitting has a maximum in a girdle normal to X with anisotropy of 5 to 8%. Calculations near the phase transition at a pressure of 48 GPa for CPO with easy <110>{1$\bar{1}$0} and [001] systems showed similar patterns to those at 21 GPa except that S wave anisotropy was stronger (11-18%). In conditions at the phase transition where <110>{1$\bar{1}$0} are the only easy glide systems, the seismic properties are very different, with Vp almost isotropic with anisotropy of 1.8% and a relatively low anisotropy of S waves with a maximum shear wave splitting of 4.5% in a single peak parallel to Z.

Key-words: stishovite, dislocations, high pressure, plastic deformation, elastic instability, seismic properties, vico-plastic modelling, CPO.

1. Introduction

In the Earth's interior, stishovite is the stable form of free SiO_2 at pressures of the transition zone and of the top of the lower mantle to a depth of 1200 to 1500 km. Although free SiO_2 is not expected to be a significant constituent in a homogeneous pyrolitic mantle, it might be present in subducted MORB's (Ringwood, 1991). Moreover, stishovite is an important high-pressure mineral as a prototype phase having octahedrally coordinated silicon. Stishovite was first synthesized in the laboratory by Stishov & Popova (1961). Natural occurrences were later discovered in shocked specimens from terrestrial impact structures such as Meteor crater (Chao *et al.,* 1962), Ries crater (Shoemaker & Chao, 1961; Chao & Littler, 1963) and the Vredefort (Martini, 1978). The crystal structure of stishovite, determined by Sinclair & Ringwood (1978), is a rutile-type structure with space group $P4_2/mnm$ in which the silicon is octahedrally coordinated to oxygen. The Bravais lattice of stishovite is tetragonal and the lattice parameters are a = b = 0.418 nm and c = 0.26678 nm (Ross *et al.,* 1990). The SiO_6 octahedra form edge-shared chains along the c-axis that are each connected to four other parallel chains. Polycrystalline stishovite is known to be a superhard material and the second hardest known oxide after the high-pressure phase cotunnite-structured TiO_2 (Dubrovinsky *et al.,* 2001) with a hardness of 32 GPa, hence its rheological properties are of great interest to materials and Earth sciences.

At ca. 50 GPa (at room temperature) stishovite undergoes a second-order phase transition to a $CaCl_2$ structure (Tsuchi-

DOI: 10.1127/0935-1221/2004/0016-0387
0935-1221/04/0016-0387 $ 5.85

da & Yagi, 1989; Andrault *et al.,* 1998, Carpenter *et al.,* 2000). This phase transformation corresponds to a symmetry change from $P4_2/mnm$ to orthorhombic *Pnnm*, which only involves a slight tilting of the SiO_6 polyhedra. The $P4_2/mnm$ to *Pnnm* transition is associated with a mechanical instability as suggested by *ab initio* structure calculations (Lee & Gonze, 1977) and by observed softening of the Raman B_{1g} mode (Kingma *et al.,* 1995). Based on a Landau free energy expansion, Carpenter *et al.* (2000) also suggested that the transition is accompanied by elastic anomalies. In particular, Carpenter *et al.* (2000) showed that the shear modulus (Reuss or Voigt bounds) exhibits a marked softening in the vicinity of the phase transition. This may have direct consequences for plastic deformation close to the transition. Indeed, recent x-ray diffraction experiments performed by Shieh *et al.* (2001, 2002) in the diamond anvil cell have shown a significant decrease in the differential stress supported by stishovite in the vicinity of the phase transition. Kingma *et al.* (1995) and Karki *et al.* (1997) have suggested that the transformation of the highly elastically anisotropic SiO_2 polymorphs stishovite to $CaCl_2$ structure at 50±3 GPa at room temperature may be the possible explanation of reflectivity in the top of the lower mantle. Kingma *et al.,* (1995) have estimated the $P4_2/mnm$ to *Pnnm* transformation would take place at 60 GPa at lower mantle temperatures in the range 2000 to 2500 K, corresponding to a depth of 1200-1500 km. Kawakatsu & Niu (1994) and more recently Vinnik *et al.* (2001) have observed seismic reflectivity in the lower mantle which may be explained by the SiO_2 phase transformation.

To clarify the mechanisms responsible for the behaviour observed by Shieh *et al.* (2001, 2002), we have carried out the first deformation experiments of stishovite at high pressure and high temperature in the multianvil apparatus. The dislocations and slip systems activated in this mineral are characterized by Transmission Electron Microscopy (TEM). In a second stage, we calculate the elastic energy of the various slip systems that exist in stishovite as a function of pressure. This enables us to model the effect of the elastic instablity at the transition on the plastic properties. Based on this estimates of the active slip systems, we calculate the crystal preferred orientations of a deformed aggregate using a visco-plastic self-consistent model. The seismic properties of the deformed aggregate are finally derived.

2. High-pressure deformation experiments

2.1. Experimental procedure

Routine deformation experiments can be performed in the multianvil apparatus at pressures up to 25 GPa and temperatures up to 2100°C. In a previous study, Cordier & Sharp (1998) have shown that <100>, [001], <110> and <101> dislocations are present in polycrystalline stishovite samples, synthesized in a multi-anvil apparatus at 15 GPa and 1200°C. However, these dislocations are likely to include growth defects and may not be representative of the easy slip systems of stishovite under mantle conditions. Cordier & Rubie (2001) have shown that deformation experiments could be performed in this pressure-temperature range by converting the hydrostatic environment of the specimen assembly to non-hydrostatic. In the present study the sample was first synthesized in a standard (nominally hydrostatic) multianvil experiment from a wet silica glass. The glass core was placed in a rhenium capsule and annealed for over 10 hours at 14 GPa, 1300°C in a 14 mm high-pressure assembly. The dense specimen was then recovered and placed in a second 14 mm assembly designed to induce plastic deformation (Fig. 1), and compressed again. The deformation conditions were 14 GPa and 1300°C, for one hour. After the deformation experiment, the specimen was recovered and doubly polished thin sections were prepared for TEM.

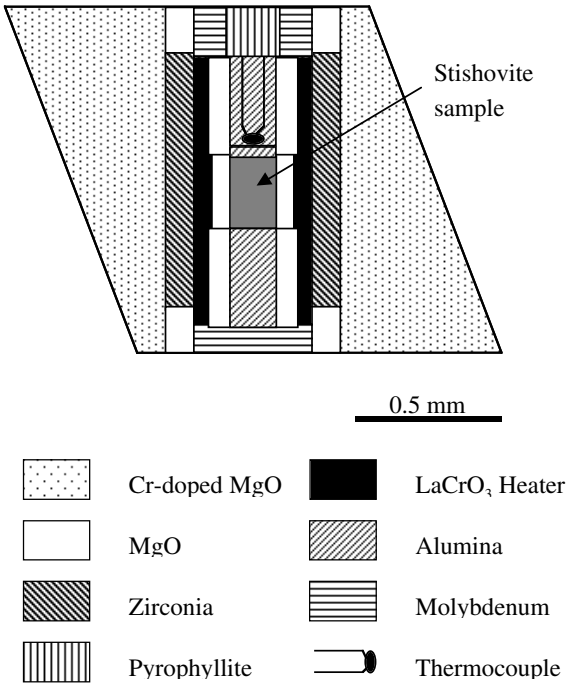

Fig. 1. Schematics of the 14 mm octahedral high-pressure deformation assembly used in the multianvil apparatus. Differential stress results from the two hard alumina pistons placed on both ends of the specimen.

2.2. Microstructural characterization and deformation mechanisms in stishovite

Optical examination of the thin sections shows that two deformation mechanisms have been activated in this sample: deformation twinning and dislocation creep (the latter mechanism is suggested by undulose extinction). Deformation twinning will be discussed in another paper, we will focus here on dislocation activity only. At the TEM scale, all grains show pervasive evidence for dislocation activity (Fig. 2). Most of the dislocations have [001] Burgers vectors as confirmed by Large Angle Convergent Beam Electron Diffraction (LACBED see Cordier *et al.* (1995) and Cordier & Sharp (1998) for more details about this technique). These [001] dislocations are found to glide in {100} and {110} planes. Dislocations in {100} are mostly screws

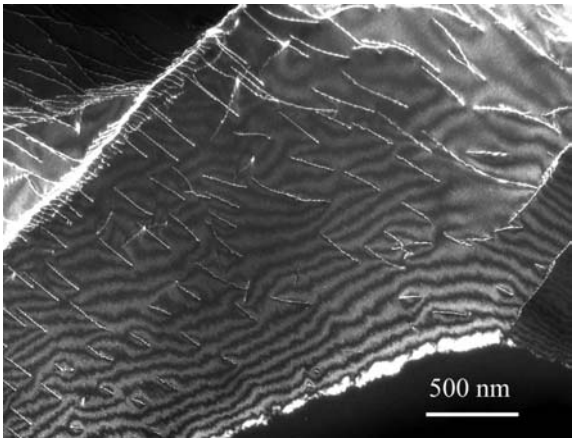

Fig. 2. [001] screw dislocations gliding in (100). Weak-beam dark-field TEM micrograph, g: 002.

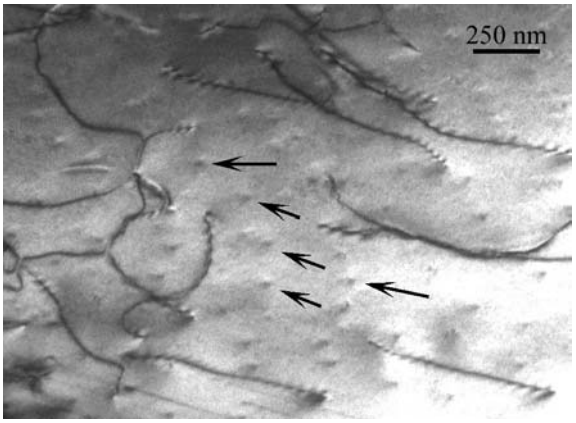

Fig. 3. <100> dislocations. Residual contrasts (arrowed) correspond to [001] dislocations. Bright-field TEM micrograph, g: 110.

whereas glide in {110} seems to be controlled by edge segments. A second kind of dislocations with Burgers vectors compatible with <100> has been observed. These dislocations were found only in grains containing a large density of [001] dislocations (Fig. 3). For this reason, their glide planes could not be identified. Glide interaction between dislocations from these different slip systems leads to the build-up of irregular subgrain boundaries. As in our previous study (Cordier & Sharp, 1998), no dissociated dislocations have been observed using weak-beam dark-field (WBDF) technique.

TEM and LACBED characterizations suggest that [001] glide is the dominant deformation mechanism in stishovite at 14 GPa, 1300°C. Stishovite has a tetragonal structure with large differences between a and c lattice parameters (c/a = 0.643 at 15 GPa). The predominance of [001] dislocations is thus consistent with the fact that these dislocations have the lowest elastic energies (the elastic energy of a dislocation line is roughly proportional to μb^2 where μ is the shear modulus and b is the Burgers vector's modulus, see the next section for more details). [001] dislocations are found to glide in the densely packed planes of the structure: {100} and {110}. The dislocations exhibit preferred line orientations corresponding to edge dislocations in the {110} planes and to screw dislocations in {100}. The origin of the preferred line orientations is probably related to contrasting mobilities related to the core structures of the dislocations. [001] screws in {100} and [001] edges in {110} are probably the dislocations which bear the largest lattice friction. This lattice friction might be due to some degree of sessile dissociation of the dislocations, however, no evidence for dissociation could be found in the TEM using WBDF. This means that either the dislocations are not dissociated, or the partial separation is below the resolution in WBDF (10-15 nm).

A single slip direction does not satisfy the Von Mises criterion for strain compatibility for plastic deformation of a polycrystal. In this respect, it is not surprising to find dislocations with Burgers vectors of the <100> type, although they exhibit higher elastic energies than [001] dislocations. <100> dislocations are usually found in grains that contain a high density of [001] dislocations, *i.e.* in grains that are strain-hardened. It is thus likely that <100> slip is characterized by a larger critical resolved shear stress than [001] slip.

Finally, the observed microstructure shows no evidence for dislocation climb. The subgrain boundaries observed are not equilibrated and probably formed through interaction of intersecting slip systems in pure glide.

Altogether, these observations suggest that at 14 GPa, 1300°C, stishovite deforms by dislocation glide. The easy slip systems are [001]{100} and [001]{110} although secondary slip along <100> is also observed.

3. Mechanical instability at the stishovite-$CaCl_2$ transition: implications on crystal plasticity

A large number of mechanisms have been proposed to account for the mechanical weakness of a material subjected to an applied stress while it is undergoing a solid-state phase transformation (Poirier, 1982; Meike, 1993). The specific case of phase transformations associated with a drop in shear modulus has been discussed by Poirier (1982). He remarks that the critical length for activating a Frank-Read source varies as μ/σ and that a drop in modulus increases dramatically the dislocation density, causing an extra creep rate. Stishovite represents an interesting case study, because, beyond the elastic instability, the stishovite-$CaCl_2$ transition corresponds to a slight orthorhombic distortion of the tetragonal unit cell of stishovite. The change of lattice parameters associated with this phase transition is modest (Andrault *et al.,* 1998). Provided that there are no drastic pressure-induced changes of the dislocation core structures (which cannot be verified at present and must be taken as a working hypothesis), one can speculate that the dislocation stabilities and slip systems should not be strongly affected by the phase transition from the crystal chemistry point of view.

We will now examine the possibility that the easy slip systems observed at 14 GPa, 1300°C are elastically weakened at the stishovite-$CaCl_2$ transition. Since the shear modulus is the relevant parameter as far as plastic deformation is concerned, it is necessary in a very anisotropic material such as stishovite to consider the elastic energy of a given dislocation line, including all the anisotropic effects. In particu-

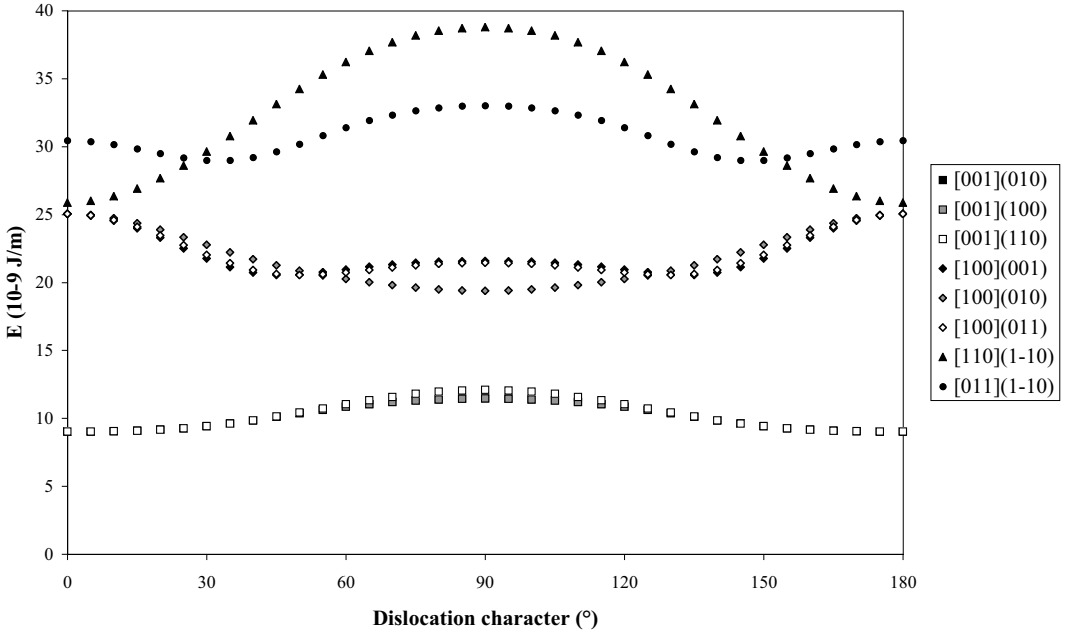

Fig. 4. Elastic energy of dislocations in stishovite at 15 GPa for several possible slip systems as a function of the dislocation character (0 and 180°: screw, 90°: edge).

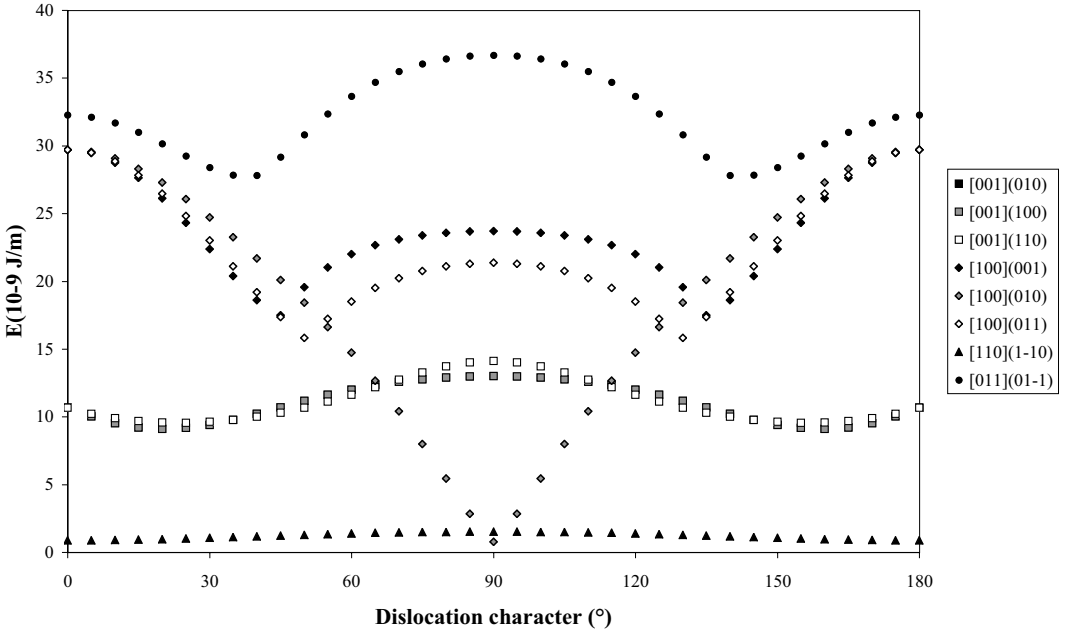

Fig. 5. Elastic energy of dislocations in stishovite at 48.9375 GPa (*i.e.* at the transition) as a function of the dislocation character (0 and 180°: screw, 90°: edge).

lar, this includes the shear modulus $\mu_{[uvw](hkl)}$ corresponding to a shear stress applied along a given [uvw] direction (parallel to the Burgers vector) within a given (hkl) plane (the slip plane). To test the influence of the elastic behaviour across the transition on the plastic deformation, we have calculated by numerical integration the elastic energy of a dislocation line using the anisotropic theory of Stroh (1958). The elastic energy of a dislocation can be considered to have two parts, one part associated with the core and the other part due to elastic distortions outside the core. From the theory of Stroh (1958) and similar methods based on classical elasticity we only have access to the non-core part of the elastic energy. Evaluation of contribution from the core is very difficult as unlike the non-core part it will change as the dislocation moves; most estimates suggest it is only 10 to 30% of the non-core elastic energy (*e.g.* Hull & Bacon, 1995). The non-core elastic energy has been calculated with DISDI. This program written by J. Douin (ONERA) allows calculation of the elastic energy as a function of the dislocation character for any crystal system, based on elastic anisotropy (Douin *et al.,* 1986). Fig. 4 presents the elastic energy (per unit length) calculated at 15 GPa as a function of

the dislocation character for several potential slip systems in stishovite. We have used the Landau theory parameterisation of Carpenter *et al.* (2000) for the stishovite to $CaCl_2$-type transformation to obtain the detailed variation of the single-crystal elastic constants and the unit-cell parameters as a function of pressure. One can see in Fig. 4 that, in good agreement with the observations made in deformed samples, [001] slip is energetically favourable. The evolution of the elastic energies as the stishovite-$CaCl_2$ transition is approached, is shown in Fig. 5. The [001] slip systems are almost unaffected by the pressure increase and by the vicinity of the transition. On the contrary, the other slip systems show marked anisotropic effects, two of them showing extreme changes. The elastic energy of $[110](1\bar{1}0)$ dislocation is found to fall to zero when the transition is approached. This variation is governed by the evolution of the anisotropic shear modulus $\mu_{[110](1\text{-}10)}$. Close to the transition to $CaCl_2$, stishovite shows that its resistance to shear along [110], parallel to $(1\bar{1}0)$ vanishes. It is worth noticing that lattice friction, that is proportional to the shear modulus, will also vanish. There is no longer any resistance to plastic shear by lattice friction and [110] dislocations can freely expand their lines at no cost. The [100](010) dislocation also show very large variations of elastic energy, with the one of edge segments falling to zero at the transition pressure. In this case, the effect is not due to a softening of the $\mu_{[100](010)}$ shear modulus as the screw segments would also be affected in that case. Pure anisotropic effects are responsible for the reduction of the energy of [100](010) edge dislocations. Having virtually no line tension, these dislocation segments are likely to expand under very small stresses although the question of their mobilities (dissociation, lattice friction,…) might be more complex and cannot completely be predicted here.

These calculations show that the elastic instability observed by Raman spectroscopy at the stishovite-$CaCl_2$ transition is likely to have major implications on the plastic properties. Dislocation line instabilities as well as anisotropic elastic softening can account for the weakening reported by Shieh *et al.* (2001, 2002). This effect is likely to be very similar to the one reported recently in quartz (Schmidt *et al.,* 2003) at the α-β transition which corresponds to a comparable elastic instability. Moreover, our calculations support the hypothesis of a change in dominant slip systems at the vicinity of the transition. Easy [001] slip should be replaced by $[110](1\bar{1}0)$ and possibly [100](010) as the $CaCl_2$ stability field is approached.

4. Self-consistent modelling of crystal preferred orientations

4.1. The self-consistent polycrystal model

The single crystal plastic properties are fundamental to our understanding of mechanical behaviour, but for geodynamical applications we are more concerned with the polycrystalline behaviour. Over the last 10 years considerable progress has been made in the modelling of polycrystalline behaviour using the dislocation slip systems determined for the majority of cases on single crystals data. The pioneering work in Earth sciences of Wenk and co-workers (*e.g.*Wenk *et al.,*1991) has established that visco-plastic self-consistent (VPSC) model, originally developed by Molinari *et al.* (1987) and extended to anisotropic materials by Lebensohn & Tomé (1993), provides a robust solution which reproduces the essential features of crystal preferred orientations of experimentally deformed plastically anisotropic minerals. Recently, this model has been successfully applied to polycrystalline ice (Castelnau *et al.*, 1996), probably one of the geomaterials with the highest plastic anisotropy, olivine (Tommasi *et al.,* 2000) and clinopyroxene (Bascou *et al.,* 2002). The VPSC provides rigorous mechanical framework for the CPO development and the mechanical evolution as a function of finite strain. Although the robustness of the model has been firmly established for CPO, the verification of the mechanical predictions has received much less attention and from the work of Castelnau *et al.* (1996) would seem less certain and more sensitive to model parameters. In what follows we will confine our attention to the model predictions of the CPO.

The VPSC model is based on three assumptions: (i) the crystals that constitute the polycrystal deform uniquely by homogeneous intracrystalline slip, (ii) individual crystals obey a viscous rheology with shear strain rate proportional to shear stress raised to a power n, and (iii) the aggregate behaviour may be calculated as a volume average of the behaviour of the individual crystals. Locally, from crystal to crystal, stress and strain are heterogeneous and crystals in an easy glide orientation deform faster than those in unfavourable hard orientations. Strain compatibility and stress equilibrium are ensured at the macroscopic scale, *i.e.* the polycrystalline stress (Σ_{ij}) and strain rate (E_{kl}) tensors are taken to be the volume average of the stress (σ_{ij}) and strain rates (ε_{kl}) tensors of the individual component crystals. The interaction between an individual crystal and a homogeneous effective medium (HEM) (*i.e.* the polycrystalline aggregate) is treated using the inclusion formalism of Eshelby (1957), where each crystal is considered as an ellipsoidal inclusion. Eshelby has shown that the ellipsoidal inclusion has the unique property of having uniform internal stress, strain and strain rate fields. The uniform stresses and strain rates of the individual crystals are thus related to the macroscopic HEM polycrystalline quantities through,

$$\varepsilon_{kl} - E_{kl} = -\alpha\, M_{ijkl}\, (\sigma_{ij} - \Sigma_{ij})$$

where M_{ijkl} is the interaction tensor which depends on the rheological properties of the polycrystal and the ellipsoidal shape of the inclusions. The constant α describes the interaction between crystals and the HEM, *i.e.* it imposes more or less stringent kinematics conditions on crystals. A zero value of α corresponds to the Taylor (1938) model (the upper mechanical bound approach) that imposes homogeneous strain on all crystals (*i.e.* $\varepsilon_{kl} = E_{kl}$) and requires that at least 5 independent slip systems are available. A value of one corresponds to the tangent VPSC model of Lebensohn & Tomé (1993), and an infinite value corresponds to the stress equilibrium model (*i.e.* the lower bound approach; Chastel *et al.,* 1993). The VPSC and stress equilibrium models can operate with less than 5 independent slip systems as locally strain compatibility is not required.

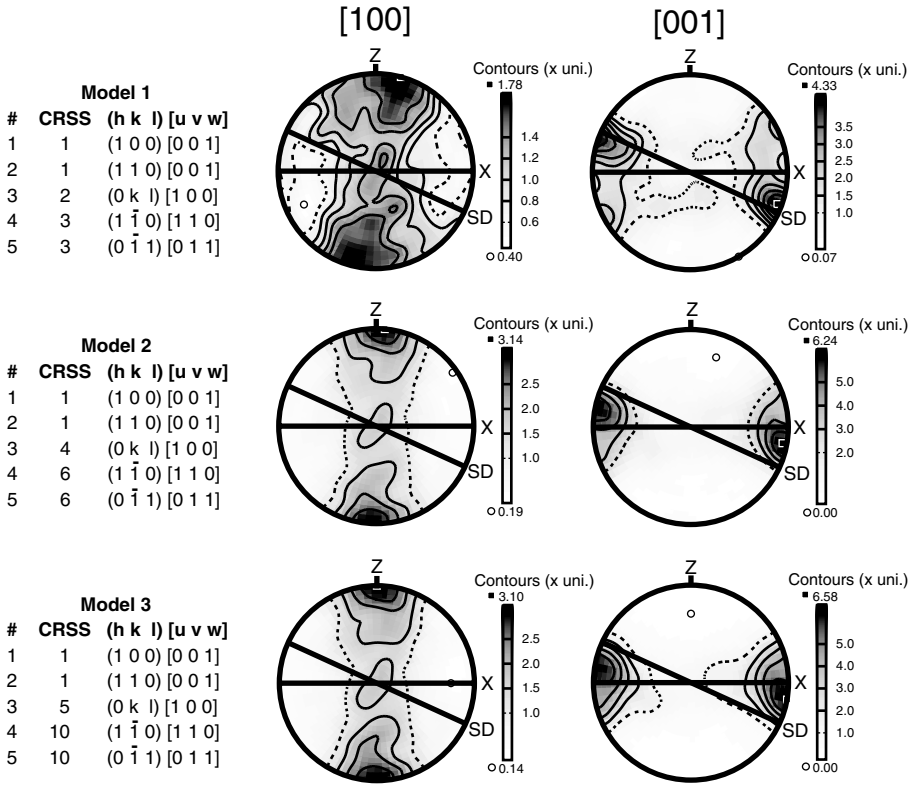

Fig. 6. Stishovite [100] and [001] pole figures for VPSC models 1, 2 and 3 far from the phase transition. X, Z are finite strain axes with X and Z being the direction of maximum and minimum extension directions respectively. The XY finite strain plane is marked by a horizontal line. SD is the shear direction in the shear plane (marked by inclined line). All plots lower hemisphere. Contours are given in multiples of a uniform distribution. Minimum contour is a dashed line

4.2. Prediction of stishovite textures

To perform a model calculation we need to define the initial CPO, initial crystal shape, interaction parameter $\alpha\Delta$, power law stress exponent (n), a constant imposed velocity gradient tensor, a set of slip systems and their relative critical resolved shear stresses. Here we have taken the initial CPO to be composed of 1000 random individual orientations with spherical shape. If non-glide mechanisms contribute significantly to the aggregate strain, for example dislocation climb or grain boundary sliding, then one could approximate this by relaxing the strain compatibility requirements provided by glide by making the interaction parameter α greater than one and hence approach the stress equilibrium model. However TEM observations did not show any evidence for dislocation climb and hence we chose the tangent model with α = 1 for all simulations. We have no information about the stress exponent for stishovite from our experiments and we have assumed a value of 3, which is typical of many minerals at high temperature. The VPSC model is not very sensitive to n between 3 and 5 and almost all minerals have stress exponents in this range. Larger values of n increase the degree of CPO for a given finite strain. A constant velocity gradient tensor for simple shear was accumulated for 40 identical steps of 0.025 equivalent strain giving a final equivalent strain of 1.0 (shear strain γ=1.73). The slip systems were determined by TEM, but the CRSS are unknown. TEM investigations suggest that <100> glide is restricted to grains that already contain a high density of [001] dislocations. This suggests that <100> slip is characterized by a higher critical resolved shear stress than [001] slip. We have set the relative CRSS for [001] and <100> at 1 and 2 respectively, meaning that stress to activate <100> is twice that of [001]. For the [001] Burgers vector the [001](100) and [001](110) slip systems are assumed to have the same CRSS. For the <100> Burgers vector the slip plane was not determined, we chose the most general solution for this slip system with <100> {0kl}. Cordier & Sharp (1998) have shown that <110> and <101> Burgers vectors are present in stishovite, the most likely slip systems are <110>(1$\bar{1}$0) and <011>(1$\bar{1}$0). These systems have not been observed in the present experiment and it is assumed that their CRSS would be higher. To estimate the CRSS, we take the stress necessary to initiate dislocation bowing or loop multiplication which is proportional to the elastic line energy per unit length. This quantity has been calculated earlier using the anisotropic elastic theory of Stroh (1958). Hence the ratio of elastic energies should be a first-order proxy for relative CRSS in the absence of direct experimental determination. This leads us to take a value of 3 for <110>(1$\bar{1}$0) and <011>(1$\bar{1}$0). We can take this a stage further to model the CPO evolution close to the phase transition by calculating the elastic energies for each system and assigning new CRSS.

The values of the CRSS for three models in the stishovite stability field are given in Fig. 6. The resulting [100] and [001] pole figures at a shear strain of 1.73 are shown in this figure. The <100> axes form a girdle distribution approximately perpendicular to the shear direction with a maximum density of X, Y, Z multiples of a uniform distribution (m.u.d.) for models 1, 2 and 3 respectively. Notice that there is not a significant difference in the distribution between the

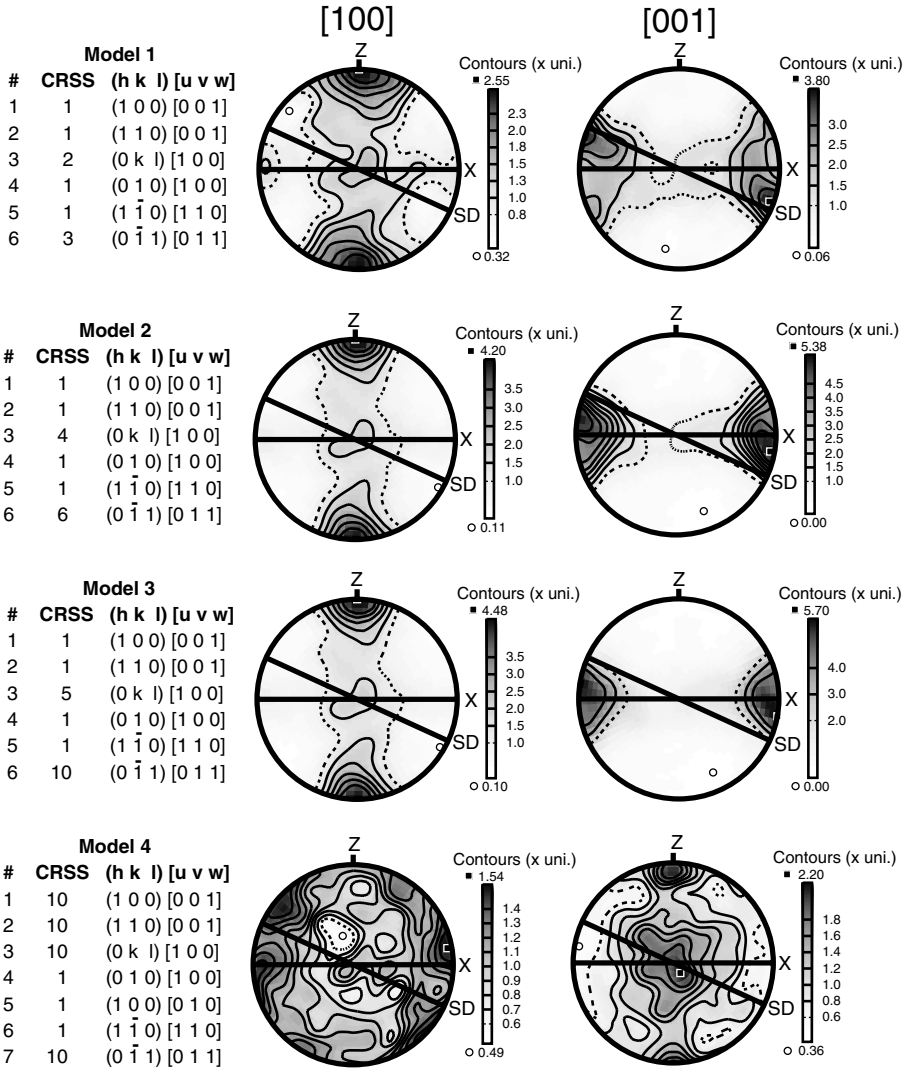

Fig. 7. Stishovite [100] and [001] pole figures for VPSC models 1, 2, 3 and 4 near the phase transition. Other details as in previous figure.

models just a slight increase of the maximum density as the ratio of CRSS of the hard systems, [100](0kl), [110](1$\bar{1}$0) and [011](1$\bar{1}$0), to the soft [001](100) and [001](110) systems increases. The [001] pole figures show point maximum close to the shear direction with a maximum density of X, Y, Z m.u.d. for models 1, 2 and 3 respectively. As for the [100] pole figures the [001] does not show a significant difference in the distribution between the models just a slight increase of the maximum density. As one might expect the easy glide in [001] direction causes a strong preferred orientation of c-axes in the shear direction.

4.3. Evolution of textures close to the phase transition

Using the anisotropic elastic energies of the dislocations we have assigned the CRSSs close to the phase transition and they are given in Fig. 7 along with the calculated pole figures. We have constructed 3 models where the [001](100) and [001](110) systems remain weak as their elastic energies do not change at the phase transformation. In addition to the weak [001] systems we have now weak [100](010) and [110](1$\bar{1}$0) systems with the same CRSS as their elastic energies decrease sharply at the transition. In models 1, 2 and 3 we have changed the relative strengths of the higher CRSS systems [100](0kl) and [011](1$\bar{1}$0) compared to the weaker systems. As shown in Fig. 7 the general distribution of crystal axes is very similar in models 1, 2 and 3, although strength of maximum [001] pole figure density increases from 3.8 to 5.4 to 5.7 m.u.d. as the CRSS ratio between the strong to weak systems increases. However, the general distribution of axes is very similar to previous models in Fig. 6 where [100](010) and [110](1$\bar{1}$0) where relatively strong. It is known that there is an experimentally observed decrease strength at the transition, hence one should observe some change in the microstructure components such as dislocation density and crystal preferred orientation. We have calculated that elastic energies of [100](010) and [110](1$\bar{1}$0) decrease to zero and are therefore significantly below the others. Also the [010](100) has a very low energy and is symmetrically equivalent to [100](010), so specifically defining that [010](100), [100](010) and [110](1$\bar{1}$0) are weakest systems at the transition and making all other systems significantly harder, we can better define a new model (4)

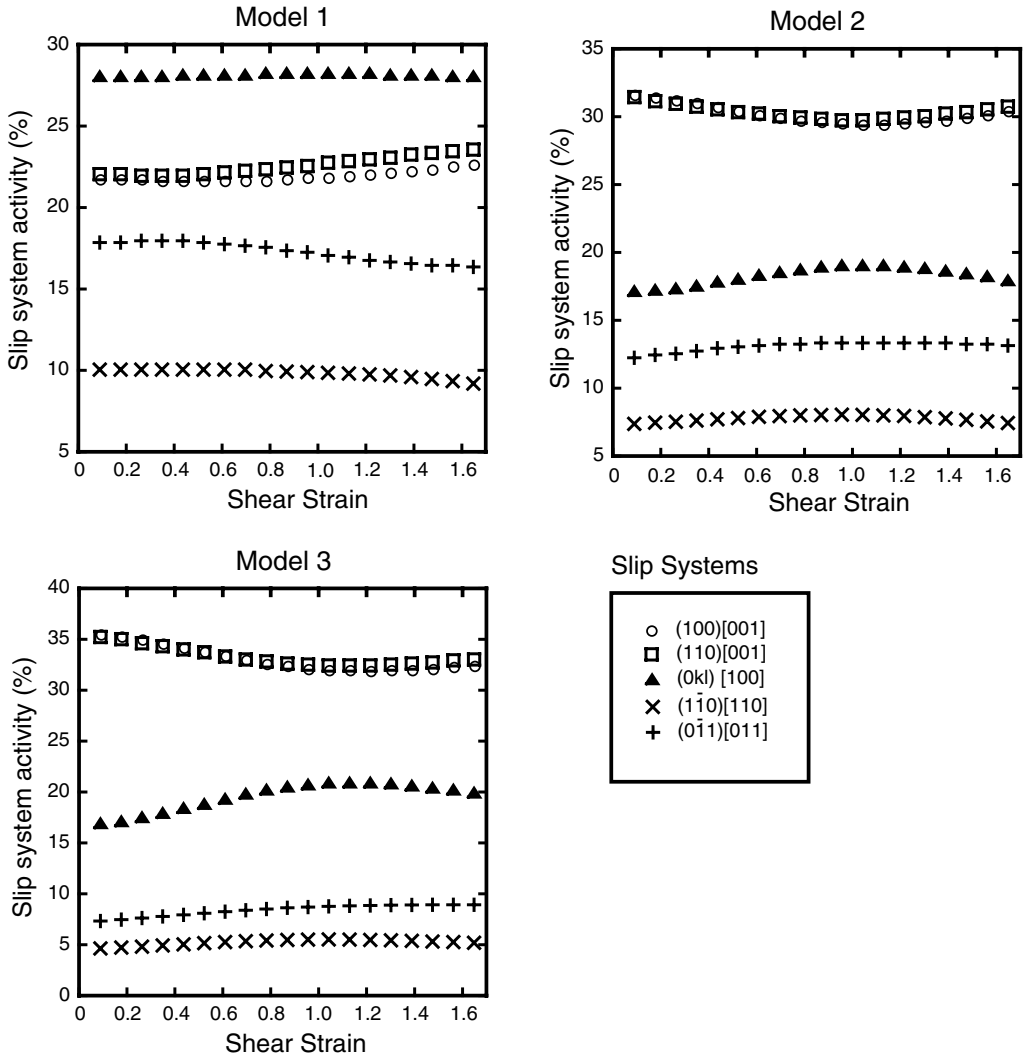

Fig. 8. Slip system activity as a function of shear strain (γ) far from the stishovite to $CaCl_2$ transition.

which takes into account that these dislocation systems become elastically unstable at the transition. The result is given in Fig. 7 and the CPO is very different from all previous models because [001] slip is no longer weak and preferred orientation has become very weak. Models 1, 2, 3 represent a situation close to the transition, whereas model 4 would be at the transition.

To further understand the development of the CPO we have plotted the glide system activity as a function of shear strain (γ) for the VPSC models far from the phase transition in Fig. 8. In model 1 the [100](0kl) appears to be dominant with an activity of about 28% of the total. One has to moderate this impression because there are of course many geometrical possibilities for slip on (0kl) planes. The activity of this system remains constant with increasing strain, whereas the weak [001](100) and [001](110) have individual contributions of 22% which increases to 24% at high strains. The combined contribution of these weak [001] systems is over 40%. The harder systems [011](1$\bar{1}$0) and [110](1$\bar{1}$0) contribute less to the overall slip activity as expected. The same pattern is repeated in models 2 and 3, but here weak [001](100) and [001](110) systems are increasingly dominant contributing 70% of the slip activity in model 3.

Near the phase transition the slip activity changes with the introduction of the 'new' weak systems [100](010) and [110](1$\bar{1}$0). The [110](1$\bar{1}$0) has a very high slip activity in models 1, 2 and 3. The [100](010) and [110](1$\bar{1}$0) both show decreasing activity with increasing strain. In contrast the [001](100) and [001](110) show increasing activity with increasing strain and eventually become the dominant systems at higher strains. In model 4 the picture is entirely different with significant activity being confined to 'new' weak systems [100](010) and [110](1$\bar{1}$0). Notice the symmetrically equivalent systems [100](010) and [010](100) have exactly the same activity and this provides an internal consistency check for the model.

5. Implications on seismic properties

There has already been some speculations on the seismic implications for the mantle of the changing elastic proper-

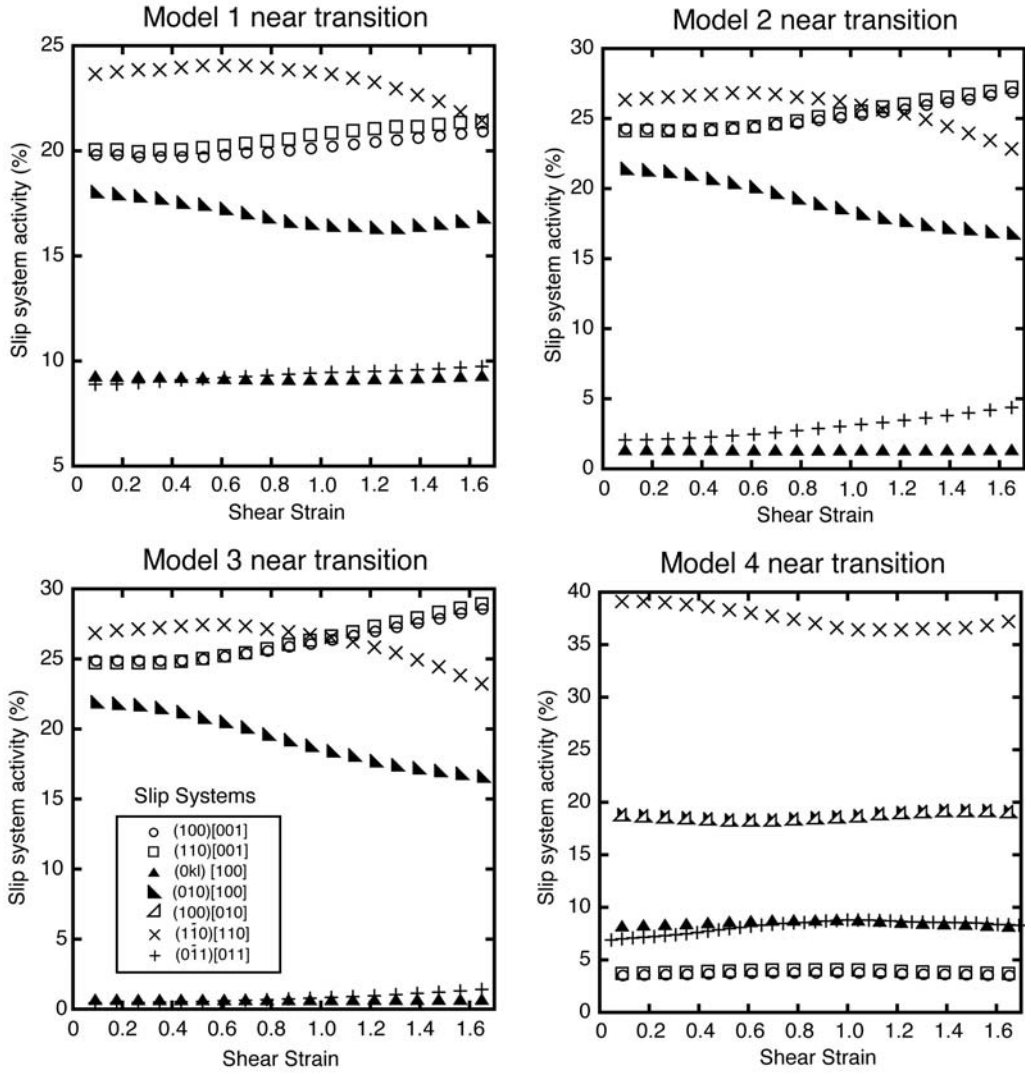

Fig. 9. Slip system activity as a function of shear strain (γ) near the stishovite to $CaCl_2$ transition.

ties around the stishovite to $CaCl_2$ transition based on the single-crystal properties (*e.g.* Karki *et al.,* 1997; Carpenter *et al.,* 2000). Using the CPO provided by the VPSC models we can calculate a predictive model for the seismic properties of polycrystalline stishovite with a CPO. Single-crystal stishovite has one of the highest seismic anisotropies of any mantle mineral, with Vp and Vs anisotropy of 27% and 36% respectively (see Mainprice *et al.,* 2000 for a review of mantle minerals).

For crystalline mantle rocks the seismic properties can be routinely calculated by making a volume-weighted average of elastic constants of the single-crystal elastic tensor in an orientation defined by the CPO. The volume-averaged elastic constants $<C_{ijkl}>$ are then used to calculate the velocities (V) and displacement directions of the three waves (P and two orthogonally polarized S) are given by the eigenvalues (velocities) and eigenvectors (displacement directions) of the second-order symmetrical Christoffel matrix T_{il} defined by the Christoffel equation,

$$|T_{il} - \rho V^2 \delta_{il}| = 0 \text{ where } T_{il} = <C_{ijkl}> \mathbf{n}_j \mathbf{n}_k$$

where δ_{il} is the Kronecker's delta, **n** is a unit vector that defines the propagation direction, and ρ is the density of the aggregate. The Christoffel equation is solved in every propagation direction at 6° intervals over a hemisphere and the resulting grid is contoured to produce the velocity pole figures. We have used the Voigt-Reuss-Hill average for $<C_{ijkl}>$ in all the results presented here.

To simulate conditions far from the phase transition and in the stishovite stability field we have used elastic constants of Karki *et al.* (1997) at a pressure of 21 GPa, corresponding to about 600 km depth. As there are not, to our knowledge, any single crystal elastic constant temperature derivatives available for stishovite, our constants are at room temperature. The density was corrected for pressure and a temperature of 1550 °C corresponding to 600 km. For the conditions close to the phase transformation, but still inside the stishovite stability a pressure of 48 GPa was used, which corresponds to a depth of 1200 km. The elastic constants of Carpenter *et al.* (2000) were used at 48 GPa as they capture details of the changes near the transition. The density was corrected for pressure and a temperature of 1770°C corresponding to 1200 km.

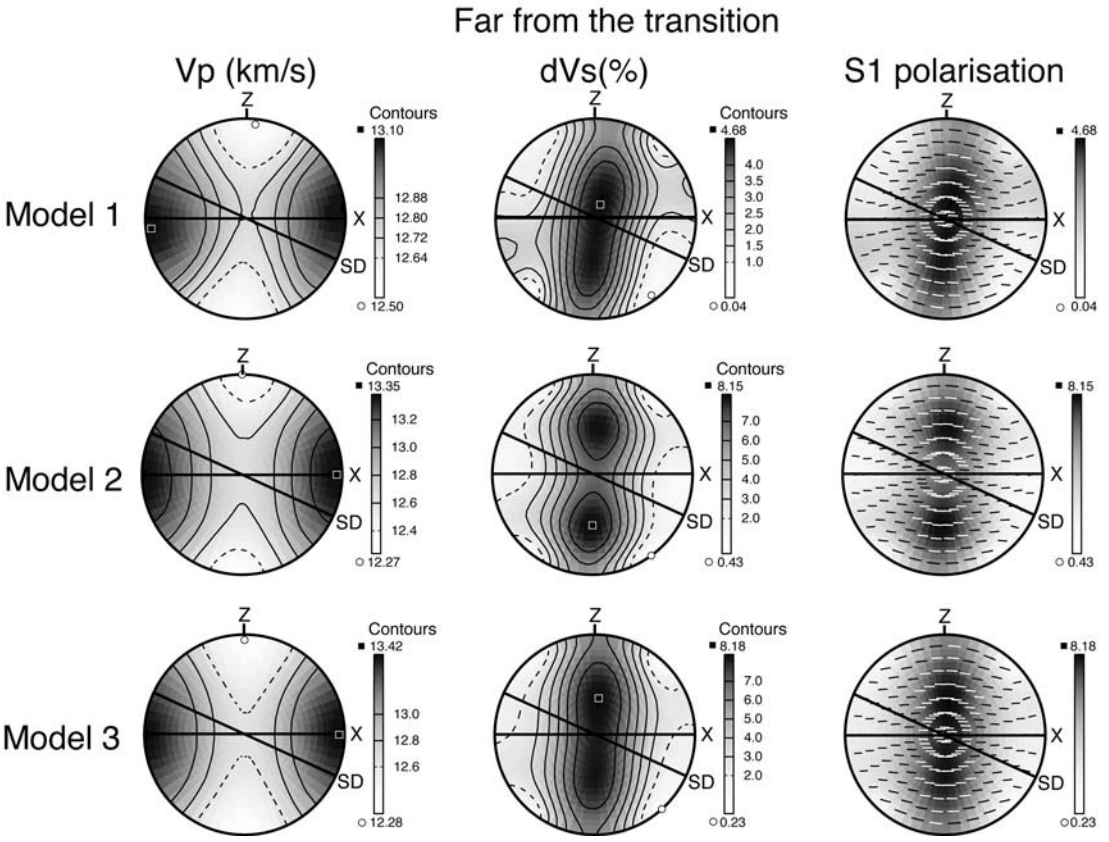

Fig. 10. Polycrystalline stishovite seismic anisotropy corresponding to the pole figures given in Fig. 6 for conditions far from the phase transition at a pressure of 21 GPa. Contours for Vp in km/s, dVs in % anisotropy and trace of the Vs1 polarization plane.

As expected, all the calculated seismic properties for the three models at a pressure of 21 GPa (Fig. 10) have a similar general pattern with high P wave velocities parallel to the maximum finite strain elongation direction X and a high shear wave splitting anisotropy normal to X. The seismic anisotropy of Vp increases from 4.7% to 13.3% to 13.4% from model 1 to 2 to 3 respectively. Similarly the S wave maximum anisotropy increases from 4.7% to 8.1% to 8.2%. Notice that models 2 and 3 are very similar. The fastest S wave (S1) polarization direction is parallel to the finite strain XY plane for all propagation directions. The general pattern is remarkably similar to that reported for olivine aggregates (see for example Mainprice *et al.,* 2000).

The calculated velocities near the transition at a pressure of 48 GPa show similar trends to those seen at 21 GPa (Fig. 11), but there are some differences. Firstly the Vp distribution is slightly different in models 1, 2 and 3 with double maximum near the X direction. The Vp anisotropy is rather lower at 4.4%, 7.0% and 7.3% for models 1, 2 and 3 respectively. The maximum S wave anisotropy (shear wave splitting) is also characterized by a double maximum about the intermediate finite strain direction Y (normal to X and Z). The orientation of the fastest S wave (S1) polarization direction is parallel to the finite strain XY plane for directions of high S wave anisotropy and normal to the XY plane for all directions of low S wave anisotropy. The seismic properties of model 4 are very different, firstly the P wave anisotropy is very low at 1.8%. Secondly the S wave anisotropy is not very high at 4.5%, but the fastest S wave (S1) polarization has no clear pattern or relationship to XYZ finite strain axes. To a first approximation we could consider model 4 to be close to isotropic.

The seismic velocity of P and S waves will gradually decrease towards the phase transition in the stishovite field and will rapidly increase in the $CaCl_2$ structure field. Seismic anisotropy in the stishovite field is also likely to decrease towards the transition. This is likely to produce seismologically observable phenomena in regions of high SiO_2 content, such as subducted MORB with 20% SiO_2 at lower mantle depths (*e.g.* Ono *et al.,* 2001).

6. Conclusions

Using a multidisciplinary approach to the plastic deformation of stishovite we have deformed a coarse-grained polycrystal at mantle pressure and temperature using a multianvil press. The active slip systems have been characterized by TEM and we have shown for the first time that [001](100) and [001](110) are dominant with secondary slip in [100] direction. These observations add to the previous identification of [110](1$\bar{1}$0) and [011](0$\bar{1}$1) in as-grown stishovite. Detailed analysis of the elastic energy of these slip systems using anisotropic elasticity theory shows that in the stishovi-

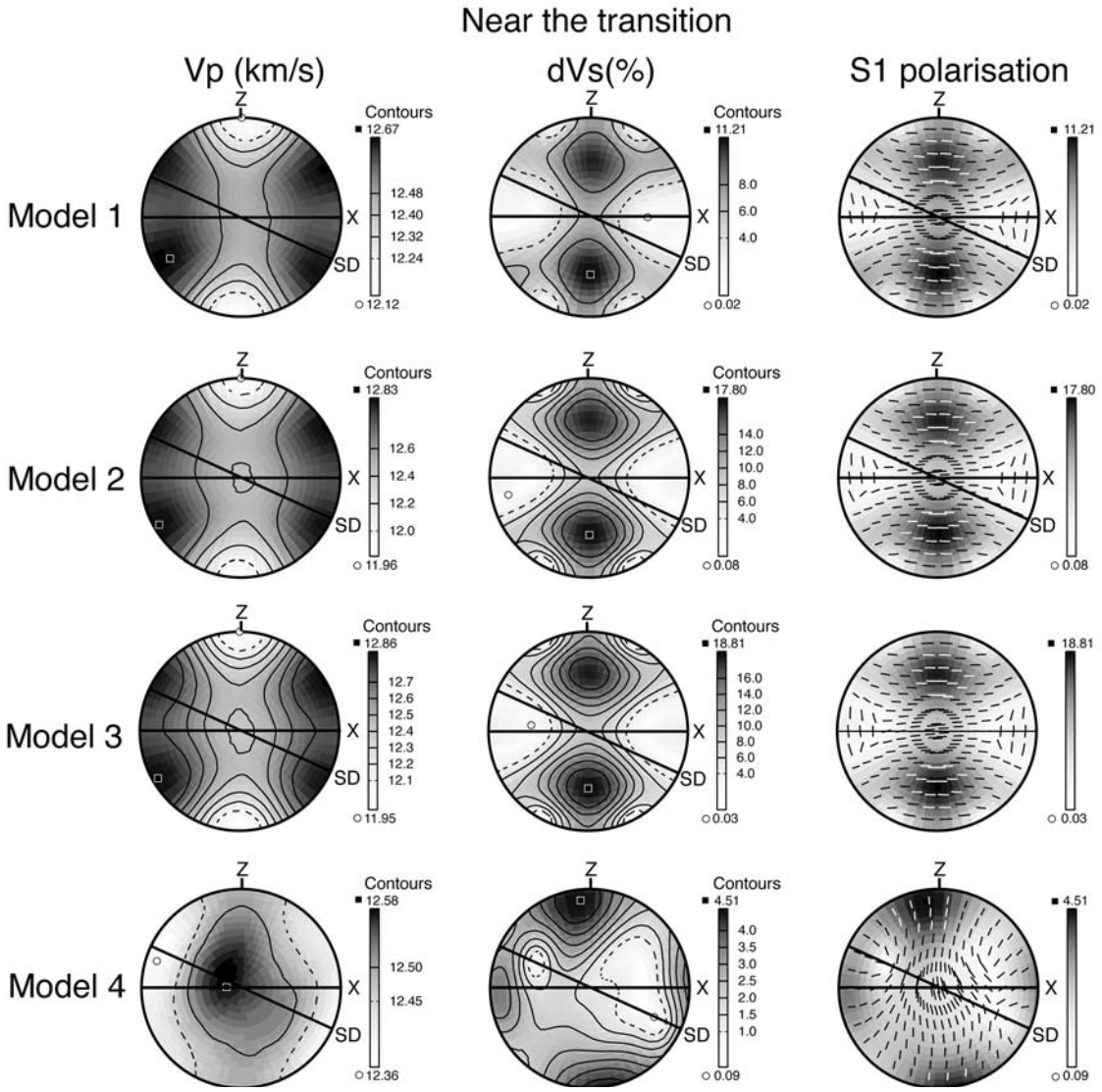

Fig. 11. Polycrystalline stishovite seismic anisotropy corresponding to the pole figures given in Fig. 7 for conditions near the phase transition, pressure of 48 GPa. Contours for Vp in km/s, dVs in % anisotropy and trace of the Vs1 polarization plane.

te stability field, [001](100) and [001](110) have the lowest energy and [110](1$\bar{1}$0) and [011](1$\bar{1}$0) have the highest, which is compatible with the TEM observation that the lower energy systems dominate the dislocation microstructure of the plastically deformed crystal and higher energy systems are present, as growth defects, in as-grown crystals. At the phase transition, elastic energy analysis reveals that energy of dislocations in the [110](1$\bar{1}$0) and [100](010) drops to near zero at the phase transition, whereas the low energy systems [001](100) and [001](110) are unaffected. The dramatic drop of elastic energy is characteristic of a plastic instability where [110](1$\bar{1}$0) and [100](010) will glide freely at very low deviatoric stresses.

The CPO of polycrystalline stishovite has been modelled using the observed slip systems and the VPSC scheme for simple shear deformation. In the stishovite stability field the predicted CPO has a strong alignment of the [001] between the shear direction and maximum finite strain axis (X) and girdle of [100] axes normal to X. The general pattern of this CPO is not very sensitive to CRSS ratio between soft and hard slip systems. Analysis of the slip system activity in the VPSC model confirms that the soft [001](100) and [001](110) systems have an increasingly dominant role with increasing shear strain. The CPO development near the transition was simulated by making [110](1$\bar{1}$0) and [100](010) soft systems with a CRSS equal to [001](100) and [001](110), the resulting CPO is very similar to the previous CPO, although slightly weaker. The slip system activity reveals that although [110](1$\bar{1}$0) dominates at low strains the soft [001](100) and [001](110) systems become dominant at high strains which explains the similarity in CPO patterns. To simulate the CPO at the phase transition the [110](1$\bar{1}$0) and [100](010) were assigned a very low CRSS and all other systems were considered to be hard, including [001](100) and [001](110). In this case a very weak CPO develops, being nearly random with weak alignment of [001] normal to

X. The [110](1$\bar{1}$0) and to a lesser extent [100](010) slip systems dominate the slip activity at all strains.

The anisotropic seismic properties have been calculated from the CPO in stishovite stability field at 21 GPa. The calculations show that Vp is maximum parallel to X and minimum parallel to Y with a high anisotropy (4.7-13.4%). For S waves the maximum shear wave splitting is in girdle normal to X with values between 4.7% and 8.2%. The polarization plane of the fastest S wave is parallel to XY finite strain plane for all propagation directions. Similar calculations made at pressure of 48 GPa to simulate conditions near the transition show similar trends to CPO with dominating [001](100) and [001](110) glide. The main differences are that Vp maximum is a double peak around X with slightly lower anisotropy (4.4-13.4%) and shear wave splitting has a higher anisotropy (11.2-18.9%) with a double peak around Y (normal to X and Z). The polarization plane of the fastest S wave is parallel to XY finite strain plane only for propagation directions with high shear wave splitting. For the CPO corresponding to dominant [110](1$\bar{1}$0) the seismic properties are completely different. The Vp maxium is now parallel to Y, but the anisotropy is very low (1.8%) so one can consider this to be isotropic for P waves. The maximum shear wave splitting is a single peak parallel to Z with an anisotropy of 4.5%. The polarization plane of the fastest S wave is normal to the XY finite strain plane for propagation directions with high shear wave splitting near Z and is generally at high angle to the XY finite strain plane.

Acknowledgements: High-pressure experiments were performed at the Bayerisches Geoinstitut under the EU "IHP – Access to Research Infrastructures" Programme (Contract No. HPRI-1999-CT-00004 to D.C. Rubie). PC has benefited from a "Congé thématique pour recherche" from the University of Lille. The quality of the preparation of the TEM specimens by H. Schultze is greatly appreciated.

References

Andrault, D., Fiquet, G., Guyot, F., Hanfland, M. (1998): Pressure-induced Landau-type transition in stishovite. *Science*, **282**, 720-724.

Bascou, J., Tommasi, A., Mainprice, D. (2002): Plastic deformation and development of clinopyroxene lattice preferred orientations in eclogites. *J. Struct. Geol.*, **24**, 1357-1368.

Carpenter, M.A., Hemley, R.J., Mao, H.K. (2000): High-pressure elasticity of stishovite and the P4(2)/mnm – *Pnnm* phase transition. *J. Geophys. Res. Solid Earth*, **105**, 10807-10816.

Castelnau, O., Duval, P., Lebensohn, R.A., Canova, G.R. (1996): Viscoplastic modelling of texture development in polycrystalline ice with a self-consistent approach: comparison with bound estimates. *J. Geophys. Res.*, **101**, 13851-13868.

Chao, E.C.T. & Littler, J. (1963): Additional evidence for the impact origin of the Ries basin, Bavaria, Germany. *Geol. Soc. Amer. Abstr.*, 127.

Chao, E.C.T., Fahey, J.J., Littler, J., Milton, D.J. (1962): Stishovite, a new mineral from Meteor Crater, Arizona. *J. Geophys. Res.*, **67**, 419-421.

Chastel, Y.B., Dawson, P.R., Wenk, H.-R., Bennett, K. (1993): Anisotropic convection with implications for the upper mantle. *J. Geophys. Res.*, **98**, 17757-17771.

Cordier, P. & Rubie, D.C. (2001): Plastic deformation of minerals under extreme pressure using a multi-anvil apparatus. *Mater. Sci. Eng. A Struct. Mater.*, **309**, 38-43.

Cordier, P. & Sharp, T.G. (1998): Large angle convergent beam electron diffraction determinations of dislocation Burgers vectors in synthetic stishovite. *Phys. Chem. Miner.*, **25**, 548-555.

Cordier, P., Morniroli, J.P., Cherns, D. (1995): Characterization of crystal defects in quartz by large-angle convergent-beam electron diffraction. *Phil. Mag. A.*, **72**, 1421-1430.

Douin, J., Veyssière, P., Beauchamp, P. (1986): Dislocation line stability in Ni_3Al. *Philos. Mag. A*, **54**, 375-393.

Dubrovinsky, L.S., Dubrovinskaia, N.A., Swamy, V., Muscat, J., Harrisson, N.M., Ahuja, R., Holm, B., Johansson, B. (2001): The hardest known oxide. *Nature*, **410**, 653-654.

Eshelby, J.D. (1957): The determination of the elastic field of a ellipsoidal inclusion, and related problems. *Proc. R. Soc. London*, **241**, 376-396.

Hull, D. & Bacon, D.J. (1995): Introduction to dislocations. Butterworth-Heinemann.

Karki, B.B., Warren, M.C., Stixrude, L., Ackland, G.J., Crain, J. (1997): Ab initio studies of high-pressure structural transformations in silica. *Phys. Rev. B Condensed Matter*, **55**, 3465-3471.

Kawakatsu, H. & Niu, F. (1994): Seismic evidence for a 920 km discontinuity in the mantle. *Nature*, **371**, 301-305.

Kingma, K.J., Cohen, R.E., Hemley, R.J., Mao, H.K. (1995): Transformation of stishovite to a denser phase at lower-mantle pressures. *Nature*, **374**, 243-245.

Lebensohn, R.A. & Tomé, C.N. (1993): A self-consistent anisotropic approach for the simulation of plastic deformation and texture development of polycrystal: application to zirconium alloys. *Acta Metall. Mater.*, **41**, 2611-2624.

Lee, C.Y. & Gonze, X. (1997): SiO_2 stishovite under high pressure: Dielectric and dynamical properties and the ferroelastic phase transition. *Phys. Rev. B Condensed Matter*, **56**, 7321-7330.

Mainprice, D., Barruol, G., Ben Ismaïl, W. (2000): The seismic anisotropy of the Earth's mantle: from single crystal to polycrystal. *In* "Earth deep interior: mineral physics and tomography from the atomic scale to the global scale", S.I. Karato, Ed. American Geophysical Union, Washington, D.C., 237-264.

Martini, J.E.J. (1978): Coesite and Stishovite in the Vredeford dome, South Africa. *Nature*, **272**, 715-717.

Meike, A. (1993): A critical review of investigations into transformation plasticity. *In* "Defects and processes in the solid state: Geoscience Applications", J.N. Boland & J.D. FitzGerald, Eds. Elsevier Science Publishers, 5-25.

Molinari, A., Canova, G.R., Azhy, S. (1987): A self-consistent approach of the large deformation polycrystal viscoplasticity. *Acta Metall.*, **35**, 2983-2994.

Ono, S., Ito, E., Katsura, T. (2001): Mineralogy of subducted basaltic crust (MORB) from 25 to 37 GPa, and chemical heterogeneity of the lower mantle. *Earth Planet. Sci. Lett.*, **190**, 57-63.

Poirier, J.P. (1982): On transformation plasticity. *J. Geophys. Res.*, **87**, 6791-6797.

Ringwood, A.E. (1991): Phase transitions and their bearing on the constitution and dynamics of the mantle. *Geochim. Cosmochim. Acta*, **55**, 2083-2110.

Ross, N., Shu, J.-F., Hazen, R.M. (1990): High pressure crystal chemistry of stishovite. *Am. Mineral.*, **75**, 739-747.

Schmidt, C., Bruhn, D., Wirth, R. (2003): Experimental evidence of transformation plasticity in silicates: minimum of creep strength in quartz. *Earth Planet. Sci. Lett.*, **205**, 273-280.

Shieh, S.R., Duffy, T.S., Li, B. (2001): Strength of SiO_2 across the stishovite-$CaCl_2$ phase boundary. International Conference on

High Pressure Science and Technology (AIRAPT-18), Beijing, China.

–, –, – (2002): Strength and elasticity of SiO_2 across the Stishovite-$CaCl_2$-type structural phase boundary. *Phys. Rev. Lett.*, **89**.

Shoemaker, E.M. & Chao, E.C.T. (1961): New evidence for the impact origin of the Ries basin, Bavaria, Germany. *J. Geophys. Res.*, **66**, 3371.

Sinclair, W. & Ringwood, A.E. (1978): Single crystal analysis of the structure of Stishovite. *Nature*, **272**, 714-715.

Stishov, S.M. & Popova, S.V. (1961): A new dense modification of silica. *Geochem. (USSR)*, **10**, 923-926.

Stroh, A.N. (1958): Dislocations and cracks in anisotropic elasticity. *Phil. Mag.*, **3**, 625-646.

Taylor, G.I. (1938): Plastic strain in metals. *J. Inst. Met.*, **62**, 307-324.

Tommasi, A., Mainprice, D., Canova, G., Chastel, Y. (2000): Viscoplastic self-consistent and equilibrium-based modeling of olivine lattice preferred orientations: Implications for the upper mantle seismic anisotropy. *J. Geophys. Res. Solid Earth*, **105**, 7893-7908.

Tsuchida, Y. & Yagi, T. (1989): A new, post-stishovite high-pressure polymorph of silica. *Nature*, **340**, 217-220.

Vinnik, L., Kato, M., Kawakatsu, H. (2001): Search for seismic discontinuities in the lower mantle. *Geophys. J. Int.*, **147**, 41-56.

Wenk, H.-R., Bennett, K., Canova, G.R., Molinari, A. (1991): Modelling plastic deformation of peridotite with the self-consistent theory. *J. Geophys. Res.*, **96**, 8337-8349.

Received 12 June 2003
Modified version received 8 December 2003
Accepted 26 January 2004